In-Flight Suppression of a Destabilized F/A-18 Structural Mode Using the Space Launch System Adaptive Augmenting Control System

John H. Wall *
Dynamic Concepts, Inc. Huntsville, Alabama 35806
(Jacobs ESSSA Group)

Tannen S. VanZwieten † and Eric T. Gilligan ‡
NASA Marshall Space Flight Center, Huntsville, AL 35812

Christopher J. Miller § and Curtis E. Hanson ¶
NASA Armstrong Flight Research Center, Edwards, CA 93523

Jeb S. Orr ‖
The Charles Stark Draper Laboratory, Inc. Huntsville, AL 35806
(Jacobs ESSSA Group)

NASA's Space Launch System (SLS) Flight Control System (FCS) includes an Adaptive Augmenting Control (AAC) component which employs a multiplicative gain update law to enhance the performance and robustness of the baseline control system for extreme off-nominal scenarios. The SLS FCS algorithm including AAC has been flight tested utilizing a specially outfitted F/A-18 fighter jet in which the pitch axis control of the aircraft was performed by a Non-linear Dynamic Inversion (NDI) controller, SLS reference models, and the SLS flight software prototype. This paper describes test cases from the research flight campaign in which the fundamental F/A-18 airframe structural mode was identified using frequency-domain reconstruction of flight data, amplified to result in closed loop instability, and suppressed in-flight by the SLS adaptive control system.

I. Introduction

NASA recently completed a comprehensive flight test campaign, the Launch Vehicle Adaptive Control (LVAC) experiment[1] to evaluate the Space Launch System (SLS) Adaptive Augmenting Control (AAC)[2,3] algorithm using a surrogate F/A-18 aircraft, the Full Scale Advanced Systems Testbed (FAST). A primary objective of the flight test evaluation was to confirm the algorithm's ability to recover from adverse control-structure interaction by responding to undesirable frequency content in the control loop. The launch vehicle dynamics were simulated for portions of the Space Launch System ascent trajectory using a dynamic inversion scheme[4] such that the Space Launch System flight software, including the adaptive element, could be evaluated during flight.

Since a subset of the F/A-18 airframe elastic dynamics are within the bandwidth of the launch vehicle control system, it was recognized that it may be possible to demonstrate this adaptive control capability

*SLS Flight Controls Lead, Guidance, Navigation, & Control Group, AIAA member
†Associate Principal Engineer, NASA Engineering and Safety Center, AIAA member
‡Aerospace Engineer, Control Systems and Analysis Branch
§FAST Chief Engineer, Flight Controls & Dynamics Branch
¶Aerospace Engineer, Flight Controls & Dynamics Branch.
‖Sr Member of the Tech Staff, Dynamics & Control

using an actual airframe longitudinal bending mode in addition to using a simulated bending response. Thus, a series of special test cases were developed and performed during the LVAC research flights. During the first series of flights, system identification maneuvers were implemented to characterize the longitudinal bending response of the FAST platform. Thereafter, a special destabilizing loop filter was designed and installed in the control path, for the purpose of driving the first airframe bending mode into a configuration susceptible to high-amplitude limit cycle oscillations. The destabilizing filter was implemented in the second series of flights using the SLS adaptive control algorithm, which demonstrated for the first time the ability of an adaptive control law to suppress undesirable control-structure interaction during flight on a manned vehicle.

In this paper, the development, test, and analysis of the elastic dynamics experiment is discussed. Background is provided in Section II. In Section III, the system identification maneuver design and analysis is presented. In Section IV, the design of a destabilizing control system configuration for the flight test is detailed. Flight test results are presented in Section V, and conclusions are discussed in Section VI.

II. Background

The LVAC flight test campaign consisted of several 60-90 minute test flights during which over 100 SLS-like trajectories were flown back-to-back at Armstrong Flight Research Center (AFRC). Each test case was configured to produce a particular SLS nominal, off-nominal, or failure scenario. The SLS FCS flight software prototype including AAC, a high fidelity reference model of the relevant SLS short-period dynamics, and F/A-18 Nonlinear Dynamic Inversion (NDI) control system[4] performed as the autopilot for the pitch axis of the F/A-18 airframe while on the SLS-like trajectories. For each specifically designed test case, the SLS FCS was executed with and without adaptation to evaluate the AAC algorithm in meeting its three main objectives:

1. do no harm (minimally adapt when not needed)
2. increase command tracking performance
3. mitigate undesirable high frequency dynamics.

Figure 1 shows the overall block diagram of the SLS FCS with the AAC algorithm encircled. The adaptive algorithm influences a well-tuned gain-scheduled Proportional-Integral-Derivative (PID) + Disturbance Compensation Algorithm (DCA) control system on a per axis basis by adjusting the total loop gain prior to the Optimal Control Allocator (OCA). The adaptive law drives smooth changes to the loop gain based upon the output of a simple reference model (increases gain), a spectral damper which discriminates high frequency content in the control path (decreases loop gain), and a modified leakage term (returns the gain to its nominal value of 1.0 when adaptation is not required).

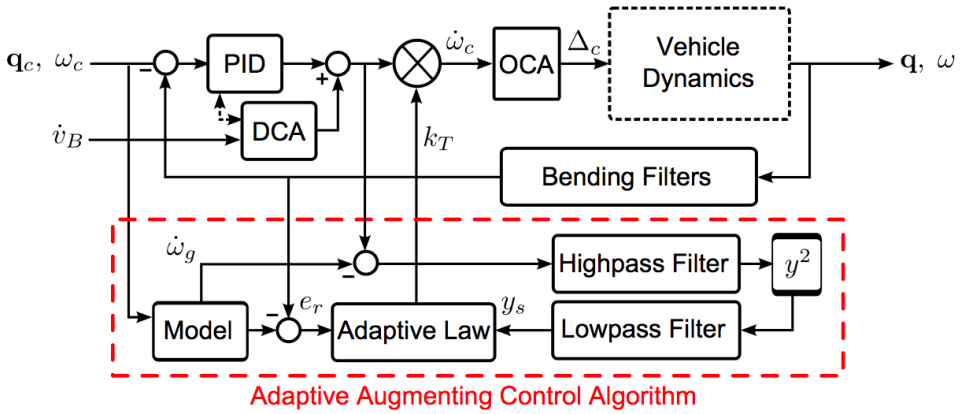

Figure 1. Block Diagram of SLS FCS with AAC

Each of the test cases flown during the LVAC experiment was developed to demonstrate one or more of the AAC objectives by configuring model, environment, and/or control to produce off-nominal but physically meaningful scenarios of varying extremity. A test case was considered successful when the multiplicative action of the AAC, according the corresponding test case objective, would yield a total loop gain that:

1. remained near 1.0 (minimal adaptation)
2. increased gain and achieved faster response to reduce excessive tracking error
3. decreased gain to stabilize or suppress parasitic high frequency dynamics

While the majority of the test cases during the flight campaign were based upon SLS data and scenarios, the series of special test cases that are the subject of the subsequent sections were developed and flown during the research flights to demonstrate the ability of the AAC to suppress an unstable control-structure interaction with the physical F/A-18 airframe. The addition of the F/A-18 structural mode test cases provided a unique opportunity to demonstrate achievement of the third AAC objective using physical structural vibration measured at the sensors.

III. Modal Identification

In the production F/A-18 flight control system, a second-order notch filter is applied in the pitch axis to provide attenuation of a fundamental structural mode around a frequency of 9.5 Hz. The same notch filter is placed on the pitch rate feedback in the experiment nonlinear dynamic inversion (NDI) flight control system to preclude any undesirable control-structure interactions. While the notch filter indicated the frequency of a fuselage mode in the control path, no additional information on the modal response of the airframe was available at the time of the experiment. To safely and accurately demonstrate an unstable but recoverable (via adaptive control) control-structure interaction, precise identification of the airframe structural response was deemed necessary. The methodology and results of this objective are described in the paragraphs that follow.

A. Methodlogy

For the first flight, a special Test Case (TC 19) was configured to excite the pitch dynamics of the aircraft over a range of frequencies where the mode was thought to exist. The result from the input excitation measured at the pitch rate feedback was then used to solve for the coefficients of a transfer function model.

To accomplish the excitation, a special programmed test input (PTI) signal was tabulated into existing tables already available for this exact purpose in the SLS controller. The PTI signal, looked up as a function of SLS trajectory time, adds a high-frequency waveform to the angular control command prior to the control allocator. Generation of the PTI waveform followed the methodology described in.[5] The PTI signal is a sum of sine waves at a specified number of discrete frequencies. The relative amplitude and phasing of the waveform is optimized to achieve a particular power distribution over the frequency spectrum and to constrain the total amplitude. This approach to in-flight system excitation was successfully employed on the Ares I-X flight test and is baselined for the first test flight of the SLS launch vehicle.

The PTI signal employed for the F/A-18 airframe modal identification test was a 20-sec waveform with a frequency range of 8 to 10.5 Hz, a resolution of 0.1 Hz, and a sample rate of 80 Hz, corresponding to the pitch axis controller update rate. The normalized amplitude time signal and the quadratic power weighting profile are shown in Figure 2.

To ensure a sufficiently long window of time for excitation and identification, the 20-sec waveform was concatenated in series three times to produce a 60-sec total waveform. Due to the constraints imposed on the end points of the original 20-sec waveform, the 60-sec version maintained continuity across the concatenation points.

A scalar gain, configurable via presses of the Nose Wheel Steering (NWS) button prior to test point engagement, was applied to the waveform before its injection into the SLS command path. The range of available gains allowed for a safe build-up approach in case the excitation levels were excessive. Additionally, this provided the ability to produce the largest excitation still within the linear range (below rate saturation) of the F/A-18 control surface actuators such that the signal to noise ratio was maximized. The gains for the excitation waveform corresponding to successive presses of the NWS button are shown in Table 1. Large valued PTI gains were required to ensure that excitation of a sufficiently large magnitude was commanded to the control surfaces since the available PTI injection point was prior to the low pass dynamics of the SLS plant model and NDI controller.

Figure 3 shows the overall system block diagram for the first round of research flights during which the modal identification TC 19 was executed. The time-derived PTI signal is shown being added between the

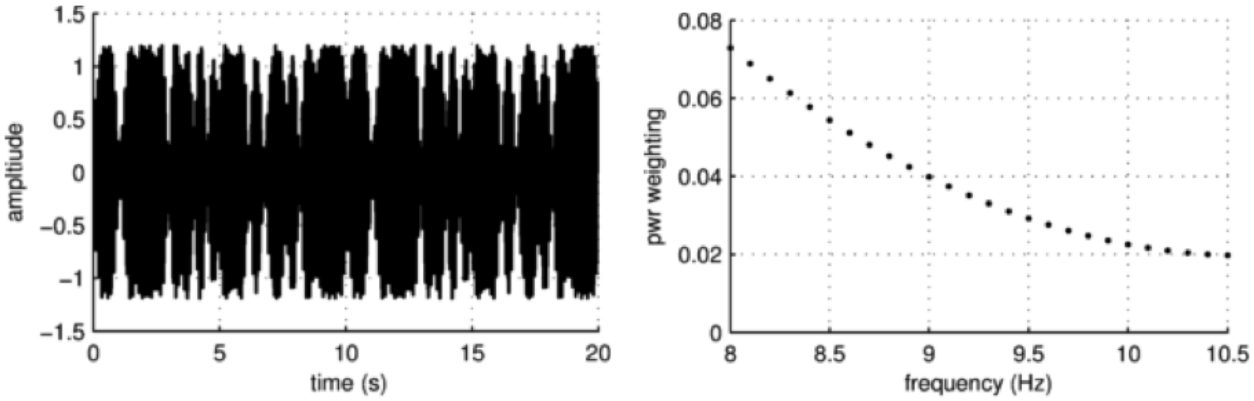

(a) Waveform (b) Weights

Figure 2. PTI Waveform and Power weighting

Table 1. In-Flight Selectable PTI Gains for TC 19

NWS	PTI Gain
0	5
1	10
2	15
3	20
4	25

SLS FCS and the SLS Optimal Control Allocator (OCA). The 9.5 Hz F-18 notch filter was maintained in the NDI feedback path but not applied to the SLS feedback paths. This was acceptable for the SLS-derived test cases since the corresponding SLS control filters (and low pass plant model dynamics) provided sufficient attenuation at 9.5 Hz. For the structural mode test cases, elimination of the notch filter from the SLS feedback to maximized the gain at 9.5 Hz for the best identification and ease of bandpass filter design.

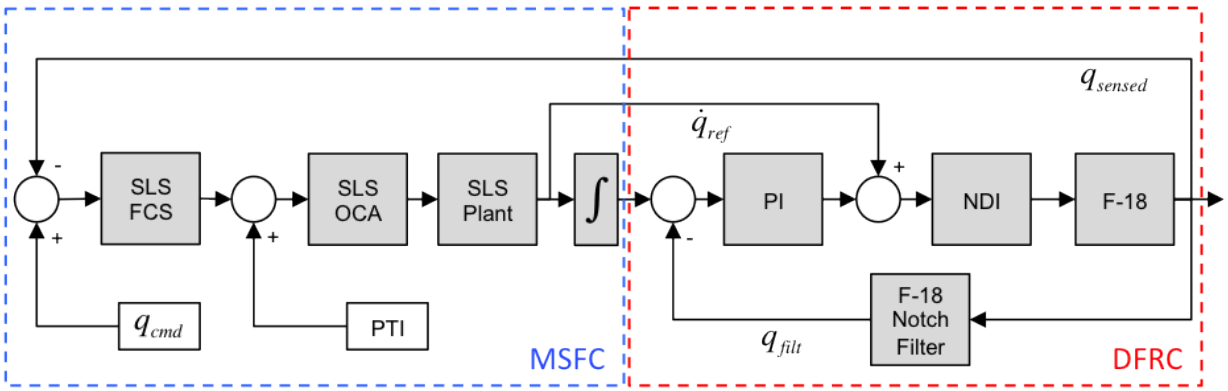

Figure 3. Test Case 19 Implementation Configuration

While the software architecture for the modal identification experiment was nearly identical to the main-line test cases, several settings were unique to TC 19:

- SLS FCS actuator position and rate limits removed.
- SLS reference model actuator model position and rate limits removed.

- SLS reference model slosh and flex dynamics disabled.
- SLS Guidance command set to fly straight and level (flight path angle and rate = 0) as the rigid body command tracking was not pertinent to the test objective.
- Wind turbulence model disabled.
- NDI control system allocated all control commands to the stabilators (as opposed to mixing with ailerons) to maximize the excitation of the fuselage mode.
- Time signal passed into the SLS plant and SLS controller was set to zero to maintain constant parameters in the SLS system.
- SLS FCS rate and attitude filters set to unity.

For the rapid development of test cases at Marshall Space Flight Center (MSFC), the entire Armstrong Flight Research Center (AFRC) NDI control system and F-18 dynamics were approximated with a third-order low pass system with input delay scheduled as a function of flight time along the trajectory. This simplification sufficiently captured the rigid body behavior of the aircraft (up to 2 to 3 Hz) and allowed the MSFC team to quickly build and test stressing SLS scenarios prior to the integration of the MSFC software (SLS FCS and plant models) into the AFRC laboratory environments (NDI and F/A-18 dynamics) and eventually flight hardware. MSFC utilized both time-domain models and linear state space models of the entire closed-loop system to develop the test cases. The time-domain models were used to produce time-history results with the time-varying nonlinear SLS plant models, SLS controller, and time-varying linear model of the NDI and F-18 attitude dynamics. The linear state space models were constructed using fixed-time parameters corresponding to the trajectory time and used to assess the stability in the frequency domain via Nichols and Bode plots.

To model the behavior of the airframe structural response around the 8 to 10Hz range, a simple second-order system with input delay was added to the output of the existing third-order system. By holding the parameters of the existing third-order system constant, the second-order system parameters were used to fit the model to flight data in the frequency range of excitation. The resulting parameters and model form were then used to derive the necessary control filter modifications and simulate the expected behavior in subsequent flights where the identified mode was intentionally destabilized and recovered with adaptive control. Equation 1 shows the form of the transfer function from the NDI angular acceleration input to the unfiltered pitch rate output. The subscript "R" denotes the third order rigid body dynamics (assumed fixed for modal identification) and "B" denotes the second order mode describing the bending dynamics observable at the rate gyro.

$$\frac{q_{sensed}}{\dot{q}_{ref}} = \frac{K_R\omega_R^2}{s\left(s^2+2\zeta_R\omega_R+\omega_R^2\right)}e^{sT_R} + \frac{K_B\omega_B^2}{s^2+2\zeta_B\omega_B+\omega_B^2}e^{sT_B} \tag{1}$$

To determine the parameters for best match, the magnitude and phase of the transfer function from the angular acceleration command into the NDI to the unfiltered sensed pitch rate was compared between the model fit and the flight data. The flight data transfer function was computed by dividing the fast Fourier transform (FFT) of the output over the FFT of the input, after applying a Hann window to the time history data. To efficiently and accurately fit the model parameters to the flight data, a MATLAB optimization routine was written to solve for the natural frequency, ω_B, damping, ζ_B, and gain, K_B, that achieved the best match. The objective for the optimization routine sought to minimize frequency integral of the squared error of the difference in Bode magnitude between the flight data and the model. The time delay, having no effect on the magnitude response, was then manually tuned to best align the phase responses.

B. Results

The FAST experiment platform includes two main inertial sensor packages available to its Airborne Research Test System (ARTS) software as shown in Figure 4. The inertial navigation system (INS) sensor package is used as the main sensor for feedback stabilization in both the production and baseline experiment control system and is mounted near the center of the fuselage. The EGI (Embedded GPS INS) sensor, located farther forward, is an auxiliary sensor providing the same data but is not used in any of the baseline critical functions. The control input for the airframe modal experiments is shown by the arrow at the rear of the

aircraft, where a force in the pitch plane is provided by deflection of the stabilators. The stabilators were allocated as the sole means of pitch control input to maximize the excitation of the structure, being located at the rear of the fuselage. Though not considered until after the first test flight (FLT 140), the EGI sensor output was obtained from the telemetry, and identification of its transfer function was pursued alongside the baseline INS. The EGI, being farther forward, gave some promise of having a higher gain at the first mode frequency and, therefore, being more readily destabilized.

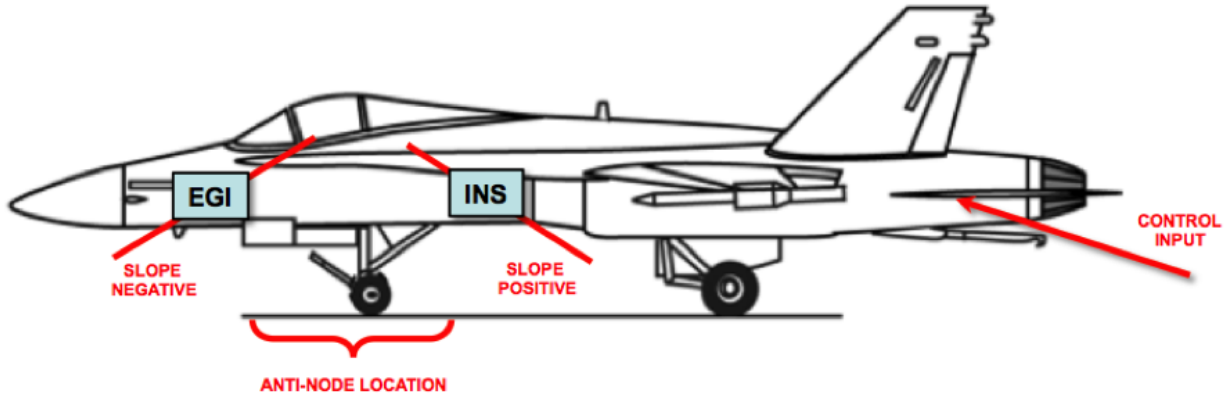

Figure 4. Airframe Sensors and Control Input

At the beginning of the first flight test (FT 140), the pilot maintained straight-and-level flight at particular speed and altitude conditions to achieve a constant dynamic pressure. The pilot then engaged the identification experiment (card 4), with the specified number of NWS button presses, and would maintain the altitude and speed with gentle stick (pitch) and throttle motions. Three such test points were flown in succession for the 60-sec duration with two (15x), three (20x), and four (25x) NWS steering presses. The data shown in the remainder of this section are derived from the three (20x) NWS presses, but similar results were obtained with using the 15x and 25x test points.

The parameters resulting from the identification of the INS and EGI transfer functions are shown in the last two columns of Table 2. These structural mode parameters fit the transfer function model of the response, with the existing rigid body parameters held at constant (t = 0) values (shown here in the first column). Of note is the sign of the gain on the two sensors. With respect to the stabilator command input, the sign of the INS is positive, where the sign of the EGI sensor is negative, with slightly higher gain. Shown pictorially in Figure 4, this indicates that for a presumed first pitch fuselage bending mode shape with a single anti-node, the anti-node falls somewhere between the INS and EGI sensors, with the EGI sensor being somewhat further from the anti-node than the INS. A single 80-Hz frame delay was necessary to model the behavior of the EGI sensor, but no frame delays were required to get acceptable phase matching with the baseline INS sensor.

Table 2. Identified Parameters for Model of Airframe Structural Mode

	Rigid Body (t=0)	INS	EGI
gain	1.0	5.33E-05	-1.24E-04
frequency (Hz)	3.36	9.53	9.41
damping ratio	0.600	0.0411	0.0348
delay (s)	0.044	0	0.0125

Figure 5 shows the raw and windowed time history data of the pitch acceleration input into the NDI and the unfiltered pitch rate from the INS sensor.

Figure 6 shows the resulting INS sensor frequency response magnitude and phase of the flight data (fft), flight data after 11 point moving average smoothing (fft smoothed), and the model fit (model). A relatively close agreement is achieved with the model parameters being especially evident with the smoothed data.

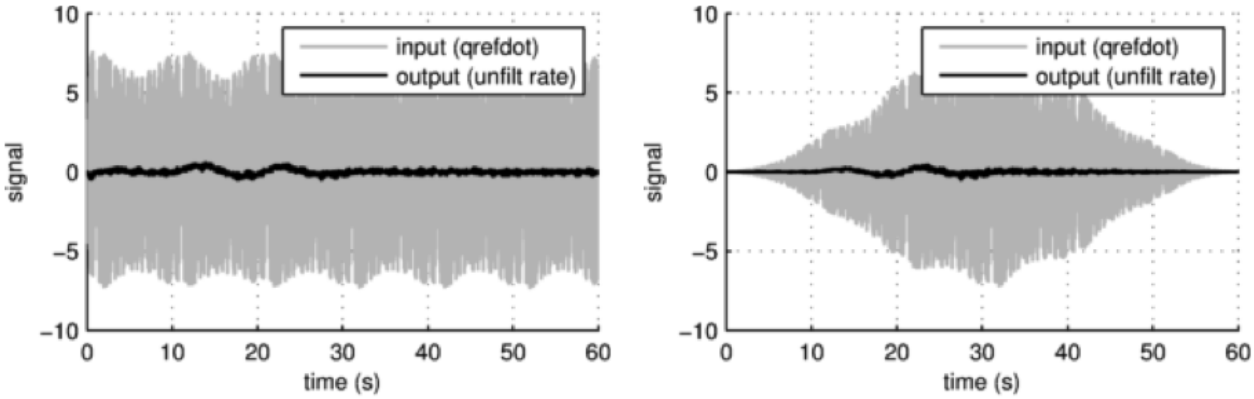

Figure 5. Raw and Windowed Time History of INS

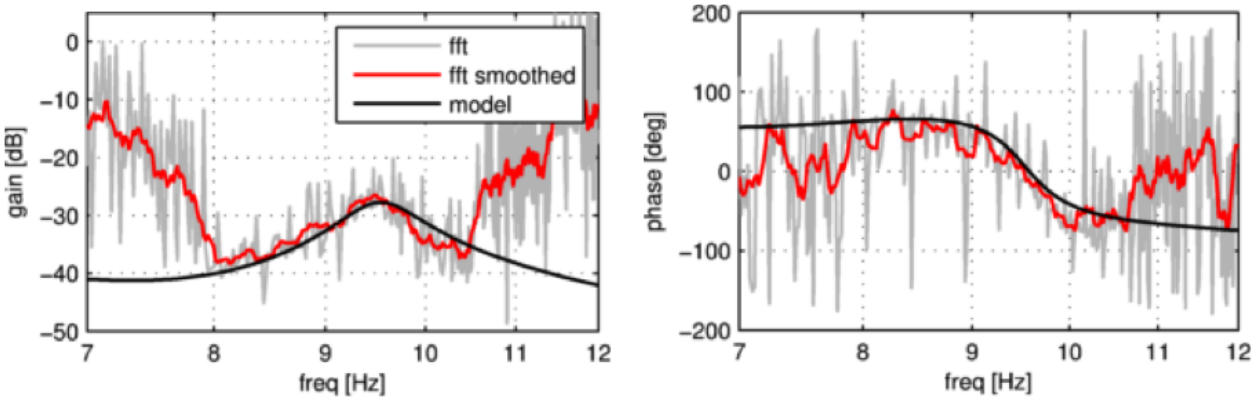

Figure 6. Frequency Response and Model Fit for INS

Figure 7 shows the resulting EGI sensor frequency response magnitude and phase of the flight data (fft), flight data after 11 point moving average smoothing (fft smoothed), and the model fit (model). A relatively close agreement is achieved with the model parameters. The raw EGI data generally exhibits more noise (or possibly aliased response data) than the INS data, but the magnitude model fit shows a good match to the flight data, especially in the smoothed response. The poorer phase mismatch in the EGI sensor results is due to the larger noise envelope causing a 180 crossing right around the frequency of the mode. The fft and fft smoothed lines are phase wrapped to +/-180 degrees whereas the model line is not. The relatively constant fft smoothed line from 9.5 to 10.5 Hz was used to determine the appropriate phase lag for the model fit. Note that the numerical optimization used the non- smoothed fft data to solve for the model parameters, and the smoothed data were used for visual verification of the fit accuracy.

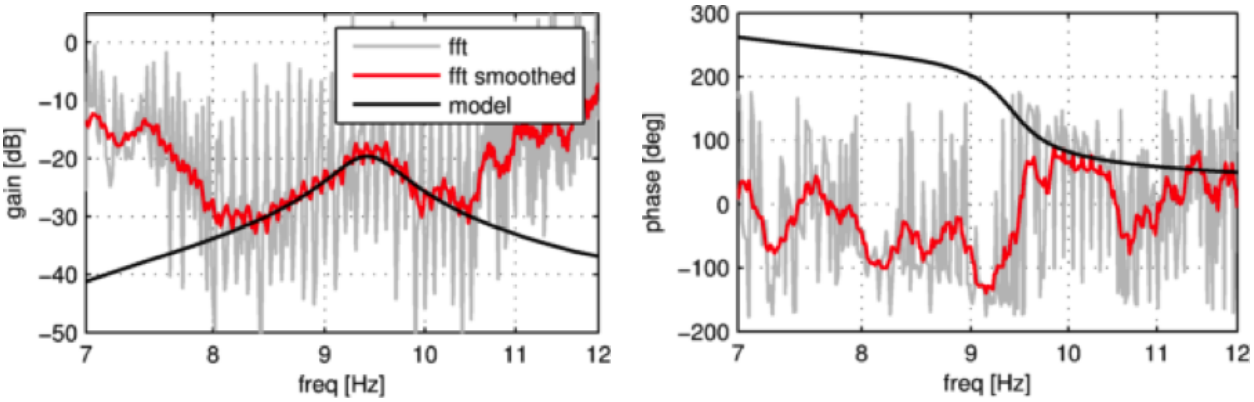

Figure 7. Frequency Response and Model Fit for EGI

The success of structural mode identification achieved through TC 19 with FLT 140 data enabled the development of the amplification test cases to accurately produce unstable mode and demonstrate efficacy of the SLS adaptive control system in mitigating its effects. The creation of these test cases are discussed in the following section.

IV. Amplification Test Case Design

After fitting the model for the response of the airframe structural mode to the flight data, TC 20 and TC 22 were created to intentionally set up an unstable control-structure interaction and demonstrate the ability of the AAC algorithm to recover the instability using the INS and EGI sensors, respectively. Filters, gains, and in-flight adjustable frame delays were applied to the control path to bring the mode to a precise amount of instability such that adaptive control had the authority (gain range) to recover. This section describes the development and setup for the amplification of TCs 20 and 22.

Figure 8 shows the block diagram configuration for the modal identification experiments TC 20 and TC 22. In contrast to the identification experiment (TC 19), the SLS OCA and plant dynamics were bypassed in TCs 20 and 22, such that the SLS control system angular acceleration command became a direct input to the NDI control system. Bypassing the plant dynamics eliminated the irrelevant SLS plant actuator dynamics in the control path and avoided having to produce the additional amplification required to uncover the resultant attenuation at the structural mode frequency. In order to achieve amplification of the airframe mode in the control path, an eighth-order bandpass filter was applied to the output of the SLS FCS along with an adjustable DC gain and frame delay. The frame delays were selectable in-flight via NWS button presses and shown in Table 3. Table 4 gives the test card options corresponding to available DC gain levels for each amplification test case. In the implementation of both sensor feedback configurations, the attitude feedback was taken from the INS sensor. As the response of the structural mode in the control path at around 9.5 Hz is dominated by the pitch rate, this was known to be acceptable approach.

The originally proposed approach to implement the bandpass filter in the SLS controller rate channel was reconsidered during testing. Filtering the rate channel would amplify sensor noise prior to the AAC, rendering it difficult to discern whether adaptation would be driven by amplified noise or actual structural resonance. Applying the bandpass filter after the SLS controller achieved equivalent control path amplification without

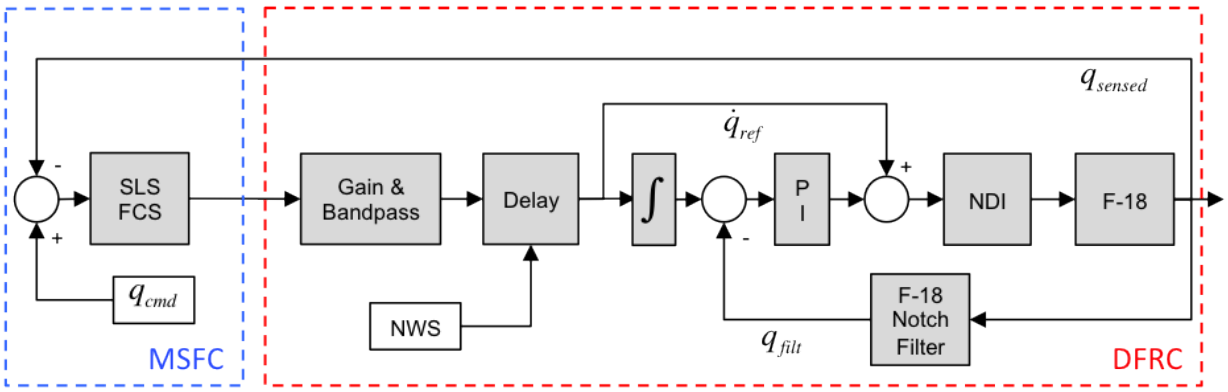

Figure 8. Amplification Experiment Configuration

Table 3. In-Flight Frame Delays for TC20 and TC22

NWS	Frame Delay	Phase Delay at 9.5 Hz
0	0 (0.0000 s)	00.00 deg
1	1 (0.0125 s)	42.75 deg
2	2 (0.0250 s)	85.50 deg
3	3 (0.0375 s)	128.25 deg
4	4 (0.0500 s)	171.00 deg

Table 4. Test Cards for Amplification Cases TC20 and TC22

Test Case	Gain	Card Number
20	-3 dB	43
	0 dB	44
	+3 dB	45
	+6 dB	46
22	-3 dB	47
	0 dB	48
	+3 dB	49
	+6 dB	50

gaining-up sensor noise on the adaptive algorithm inputs.

To ensure excitation of the modal dynamics in the otherwise quiescent straight and level flight, a short, 2-sec burst of the original PTI maneuver from TC 19 was added to the control command signal. The PTI gain was decreased to a magnitude of 0.1, a value determined from simulation sufficient to excite the modeled structural mode but without inducing significant rigid body motion or control effort.

The settings for the modal amplification TC 20 and TC 22 depart from the mainline test cases in the same respects as the modal identification TC 19 and include the following additional modifications:

- SLS OCA and plant bypassed in SLS reference model by connecting SLS flight control system angular acceleration command directly to F-18 NDI control system.
- Gain, delay, and bandpass filter applied to SLS control system output in ARTS software.
- PTI maneuver time-cropped and gained down to induce a small excitation for a short, 2-sec burst at 5 sec after the experiment engaged.

A. Modal Amplification with INS sensor

To determine the amount of amplification and phasing required by the bandpass filter for each of the test cases, the modal identification model fit parameters were installed with a unity bandpass filter, and the entire open-loop frequency response was generated. The open-loop frequency response is defined from the input into the NDI to the output of the SLS FCS, the Single-Input-Single-Output (SISO) point where the bandpass filter, gain, and delay is to be applied. Figure 9 shows the open-loop bode response when using the INS sensor for pitch rate feedback.

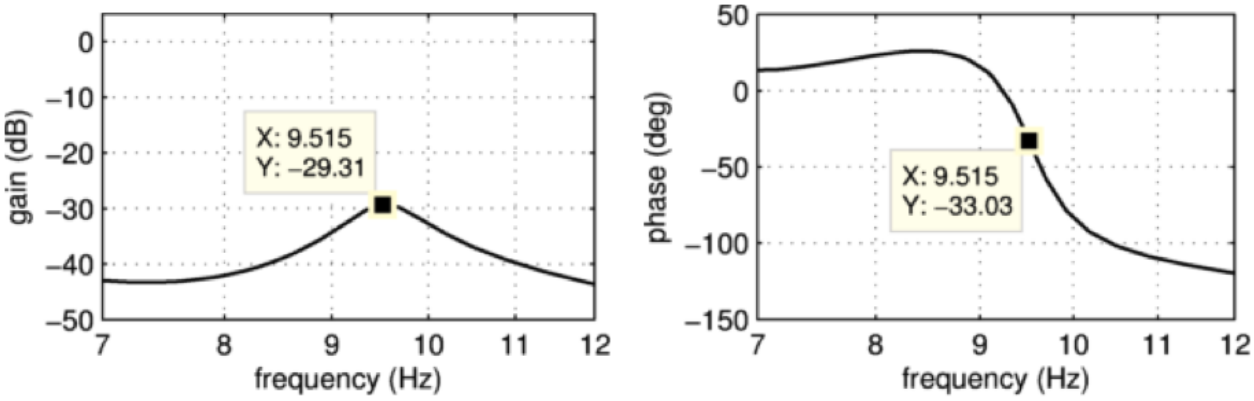

Figure 9. Open-Loop Response without Bandpass: INS feedback

The open-loop response at the peak is at approximately -29 dB of gain and -33 deg of phase. To bring the mode to instability, the required amplification is at least 29 dB and 180 - 33 = 147 deg of phase lag. Initial attempts to design an eighth-order bandpass filter that simultaneously met the gain and phase objectives proved difficult. To alleviate the phase constraints on the filter, a number of discrete frame delays were added to the path. Utilizing two 80 Hz frame delays (selectable via NWS presses in flight) provides 85.5 deg of phase lag at 9.5 Hz, which leaves 61.5 deg to be achieved with the filter.

The filter was designed utilizing the standalone filter optimization tool in the MSFC control parameter design and frequency domain stability analysis tool, FRACTAL. The methodology of the FRACTAL filter optimization tool is described in reference 6. To achieve the desired 29 dB of gain and 61.5 deg of phase lag at 9.5 Hz, gain targets and phase constraints were configured in the filter design tool which was then run to solve for the eighth-order set of coefficients to best achieve the objectives. Figure 10 shows the frequency response of the resultant filter against the magnitude targets (shaded areas) and phase constraints (red pluses). The filter amplitude and phase at the mode frequency was designed to achieve the very precise targets. The 9.5 Hz centered passband filter was specified to have unity DC gain so as to not affect the basic rigid body response or stability characteristics. At frequencies higher than the 9.5 Hz passband, attenuation is beneficial to filter out noise or any other irrelevant dynamics.

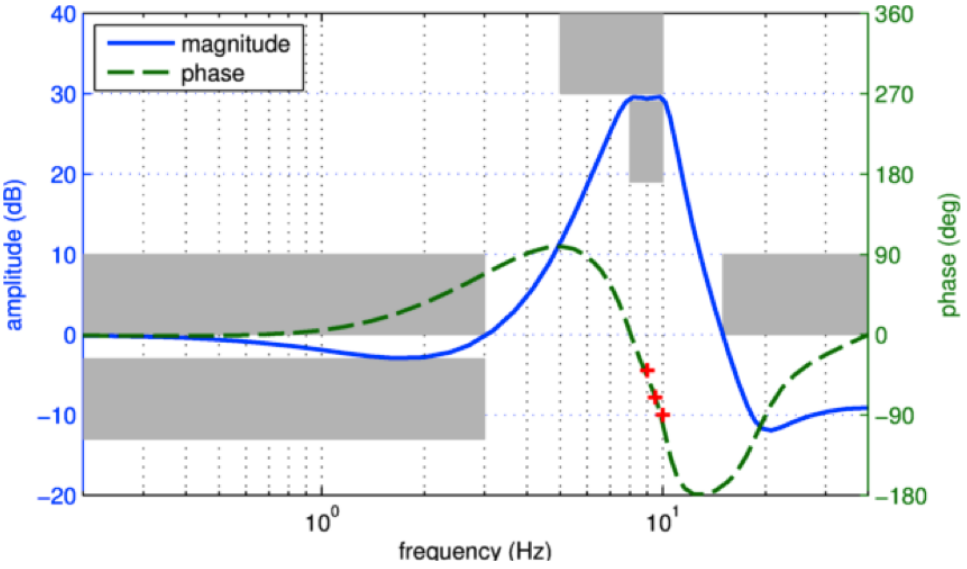

Figure 10. Bandpass Filter Response and Specifications: INS Feedback

After placing the bandpass filter in the control path and computing the open-loop response, the open-loop gain at the mode frequency is slightly above unity, but the phase lag is still 80 deg from the critical -180 degree phase point, as the filter fully constrained by the gain objectives. However, this is easily remedied by selecting two 80-Hz frame delays in flight to increase the lag to 108 + 85.5 = 193.5 deg. To further ensure an unstable mode in flight given the potential uncertainty, the test card was selected that added an additional +3 dB of gain to the control path. These two adjustments along with the filter placed the open-loop response of the airframe mode at a predicted +3.3 dB and 193.5 deg. Given the AAC gain range from -6 dB to +6 dB, the response of the system with the adjustments would have enough gain to exhibit divergence but not too much gain that AAC would be unable to decrease its gain to restore stability. Furthermore, due to the higher level of damping (4 %) of the structural mode (compared with the SLS assumed 0.5 %), the resultant gain at 180 deg for a moderate phase variation remains above 0 dB and, therefore, would result in a divergent response. In the case where the gain or phase of the mode was mismodeled or the response is higher than expected, the in-flight selectable gains and delays allowed some additional flexibility (subject to flight time constraints) toward finding the instability.

Figure 11 shows the final system as configured for test flight in which two frame delays are selected for the +3 dB test card.

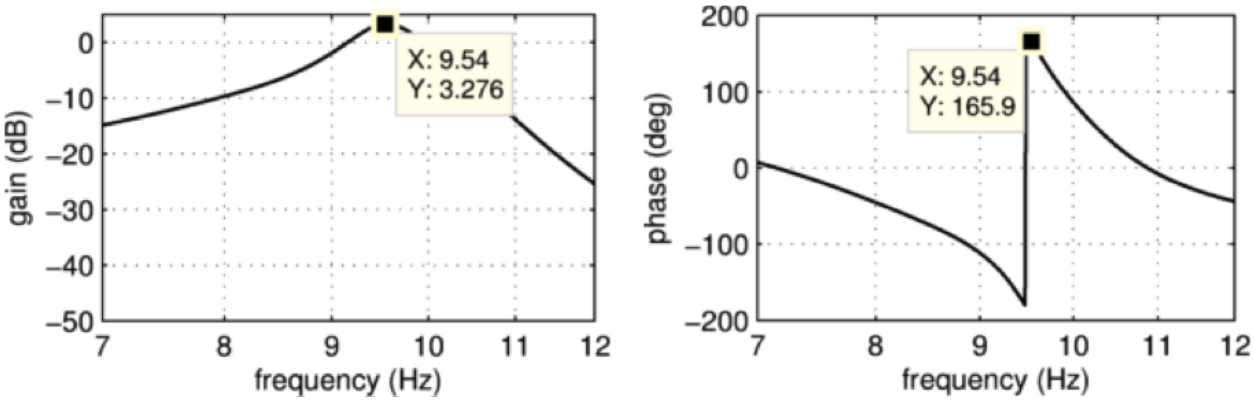

Figure 11. Open-loop Response with Bandpass Filter, Gain, and Delays Applied: INS Feedback

Figure 12 shows a Nichols chart of the open-loop response with the +3 dB gain and two frame delays configured. This depiction best illustrates the gain versus phase relationship resulting from the 4 % modal

response near the critical point: even though the magnitude peak of the frequency response does not exhibit exactly -180-deg phase (14 deg away), there is still sufficient gain at the -540 phase point (multiple of 180) to produce an instability. The Nichols plot also shows the adequate rigid body margins present in this test case configuration, even after the application of in-flight gain and phase adjustments.

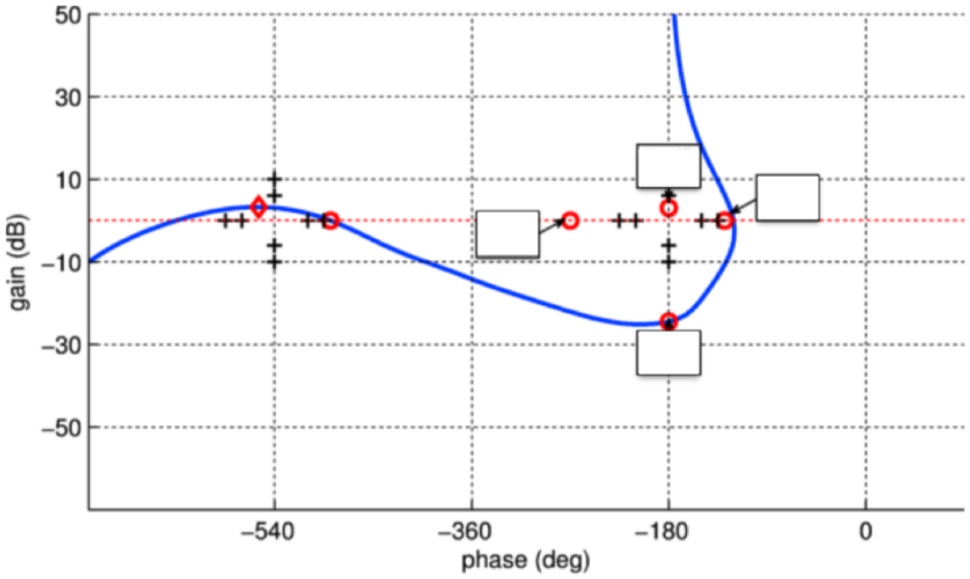

Figure 12. Nichols Open-loop Response with Bandpass Filter, Gain, and Delays Applied: INS feedback

B. Modal Amplification with EGI sensor

Following the same procedure to develop a TC for the EGI sensor feedback configuration, the EGI sensor modal identification model fit parameters were implemented in the MSFC simulation with a unity bandpass filter, and the entire open-loop frequency response was generated. The open-loop frequency response is defined from the input into the NDI to the output of the SLS FCS when using the EGI sensor for pitch rate feedback. Figure 13 shows the open-loop response with the unity filters.

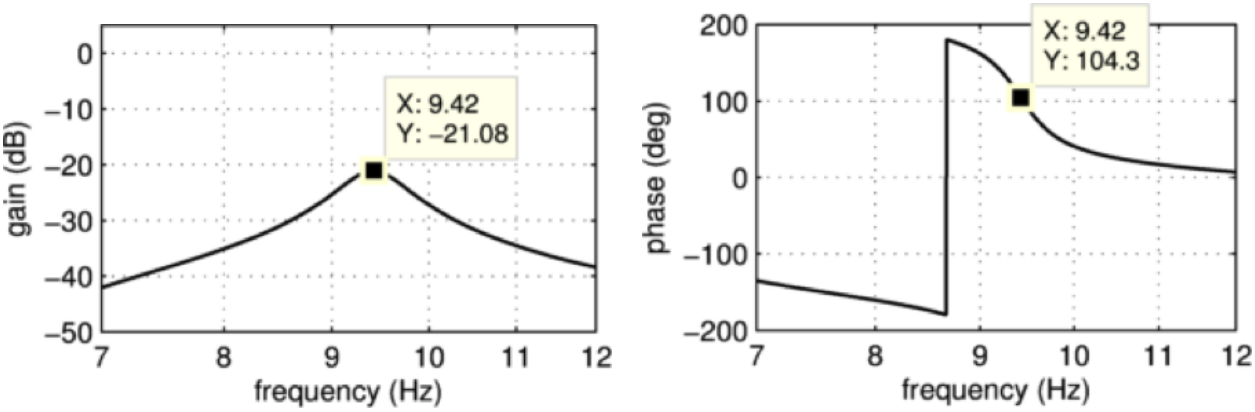

Figure 13. Open-Loop Response without Bandpass: EGI feedback

The open-loop response indicates that at least a 21 dB gain and 104.3 + 180 = 284.3 degrees of phase lag is required to destabilize the structural mode. To alleviate the phase constraints on the filter, a total of five frame delays were assumed in the open loop (corresponding to 213.75 degrees at 9.5 Hz), leaving 70.55 degrees of lag to be achieved by the bandpass filter. To utilize the same NWS schedule as for the INS feedback case and allow adjustments on either side of the nominal prediction, two fixed frame delays were added to the EGI pitch rate path for all of the TC 22 test cards.

Figure 14 shows the frequency response of the resultant filter against the magnitude (shaded areas) and phase constraint (red plus).

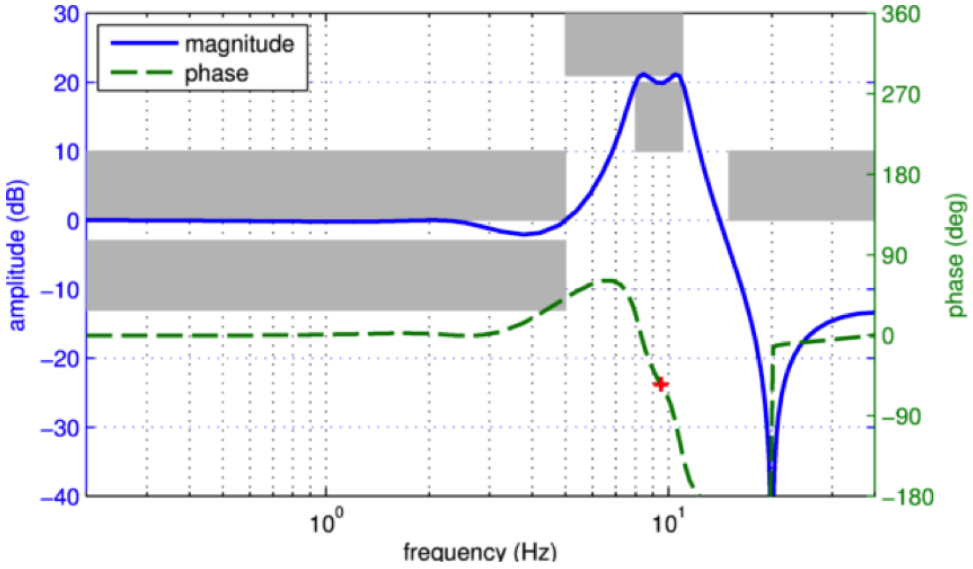

Figure 14. Bandpass Filter Response and Specifications: EGI Feedback

Figure 15 shows the open-loop Bode frequency response of the system with EGI feedback where the bandpass filter, +3 dB gain, and a total of five frame delays were applied.

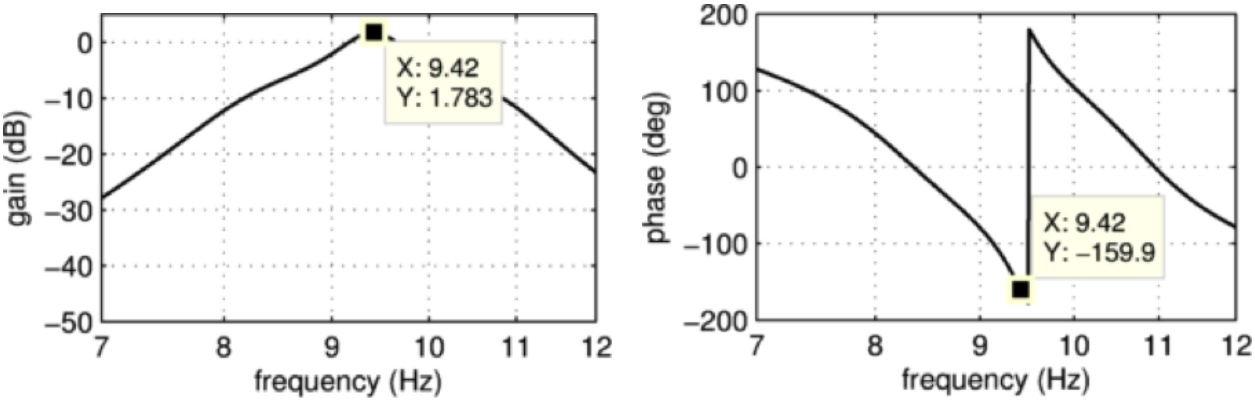

Figure 15. Open-loop Response with Bandpass Filter, Gain, and Delays Applied: EGI Feedback

Figure 16 shows the corresponding Nichols plot of the open-loop frequency response of the system with the bandpass filter, +3 dB gain, and a total of five frame delays applied. It is apparent that the gain at 900 degrees (multiple of 180) is only slightly above zero dB, indicating that, in flight, the +6 dB test card will be required to show sufficient divergence.

C. Pre-Flight Simulated Test Results (INS sensor)

Time domain results generated using the MSFC simulation for TC 20, corresponding to the +3 dB gain and two frame delay settings, are shown in Figure 17. The AAC-off (gray line) case, once hit by the short 0.1-gained PTI burst at 5 sec, exhibits an immediately divergent oscillation that grows until eventually reaching the limit of the numerical simulation. The left plots in Figure 17 show that when AAC is enabled the angular acceleration control command and pitch rate are bounded and exhibit stable behavior. The total gain (bottom right) profile, while periodic, suppresses the unstable mode by decreasing the gain and subsequently preventing divergence. The adaptive gain law also nears its lower limit of 0.5 and exhibits the predicted saturation behavior. The gain law input terms are shown in the upper right plot of Figure 17,

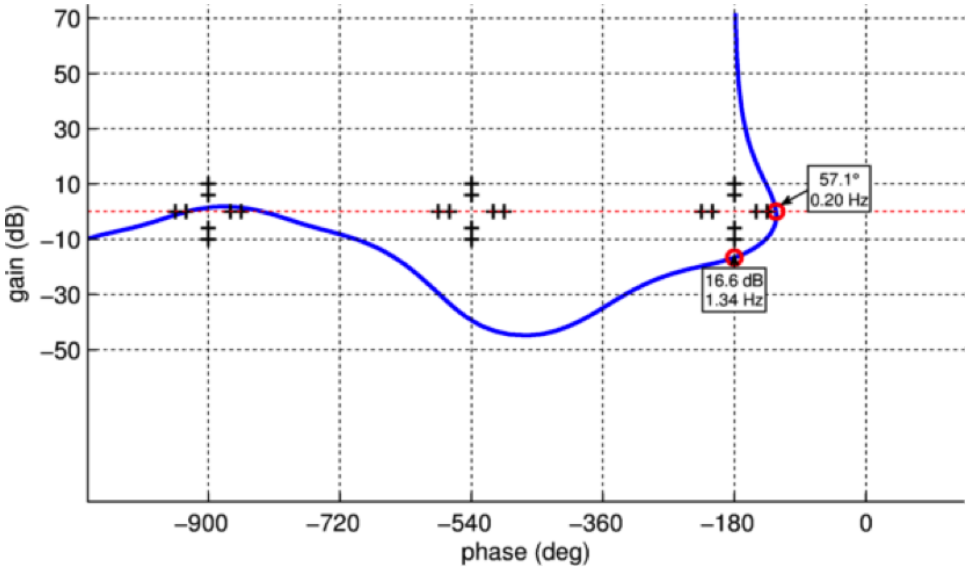

Figure 16. Nichols Open-loop Response with Bandpass Filter, Gain, and Delays Applied: EGI feedback

demonstrating the activity of the spectral damper (sdamp) driving the gain down while the leakage term attracts the gain back to unity. The reference model error term (att err) plays no signficant role in this scenario, as designed. The peaking in the spectral damper is expected due to the sudden decrease of the saturation function when the gain nears its lower limit. Since no physical limits are modeled in the MSFC simulation for this test case, the AAC-off behavior is virtually unbounded. In actual flight, the unstable mode was expected to grow until reaching the physical limitation of the actuators (to an extent not predicted prior to flight), at which point a limit cycling behavior was thought to be likely. By contrast, the AAC-on cases stay within physical limits and were expected to show similar behavior to the preflight simulations.

V. Amplification Flight Results

The structural mode amplification test cases were flown straight and level and it was therefore straightforward and desirable to fly TC 20 and TC22 cases when going out or coming home or when the pilot was required to fly to different parts of the available airspace to avoid traffic. This approach maximized achieved test points by utilizing otherwise unusable flight time, at the cost of placing the amplification test points further from the fuel level conditions corresponding to the identification test. Table 5 summarizes all of the test cases flown for the modal identification and amplification experiment, along with the fuel remaining, altitude, and speed conditions when the test card was engaged. In this section, results from the flight tests of TC 20 and TC 22 are discussed.

A. Flight Results for TC-20 (INS sensor feedback)

The first test engaged during Flight 143 was TC 20, where the airframe structural mode was amplified with INS feedback. The conditions for the gain and delay were set to the +3 dB and two-frame-delay values predicted in preflight simulation to bring the mode to a recoverable level of instability. The first test point was engaged with AAC off and soon after the PTI burst at 5 sec, a fast growth to bounded oscillation was observed in the symmetric stabilator commands. This, along with a distinct 9.5-Hz peak in the real-time Power Spectral Density (PSD) displays, demonstrated that the resultant system response at the predicted structural mode frequency was unstable. The presence of the stabilator rate limit and possibly other amplitude-dependent mechanisms of energy dissipation maintained the system response to a stable limit cycle at the resonant frequency of the airframe, and the pilot confirmed a detectable vibration in the cockpit. TC 20 was then engaged for the same conditions but with the AAC enabled. The symmetric stabilator command grew quickly to oscillation after the PTI burst, but the magnitude of oscillations thereafter continued to be suppressed by the action of the adaptive controller and were significantly less than when AAC was disabled.

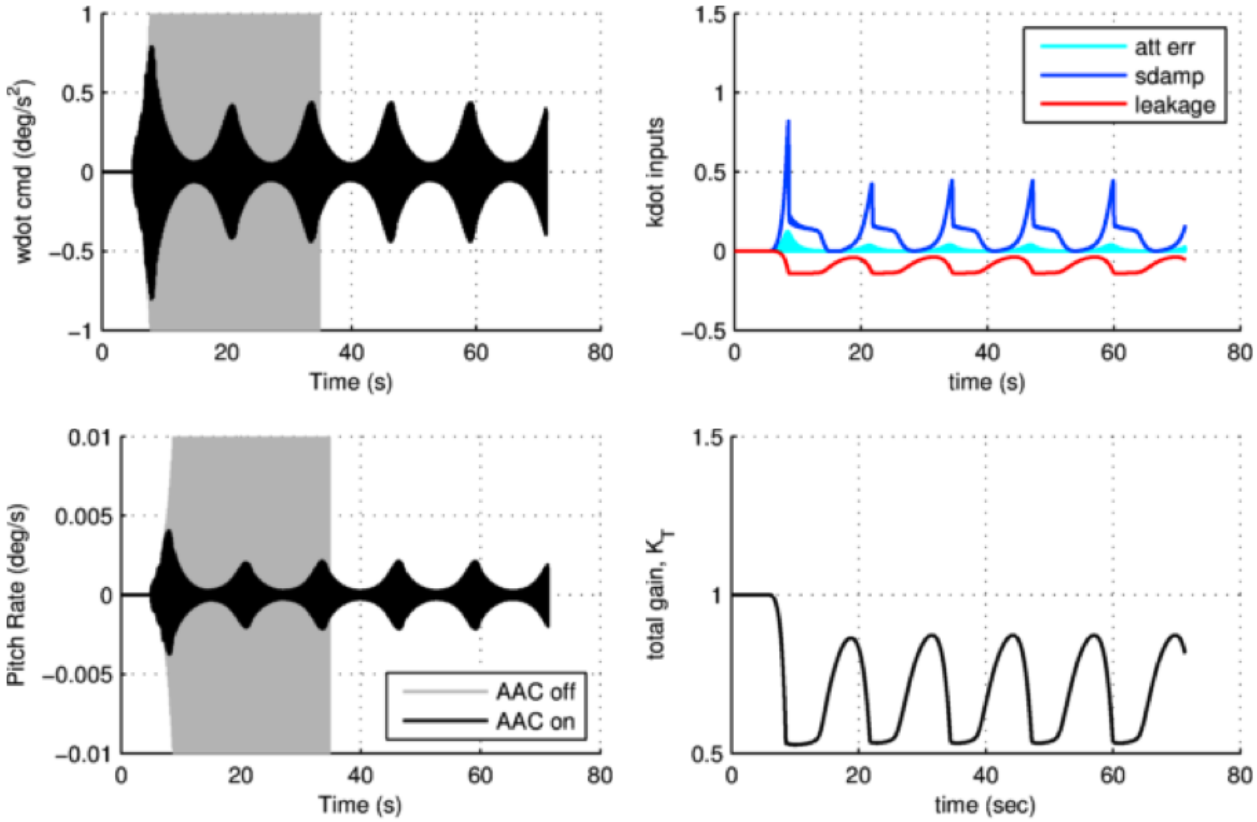

Figure 17. TC20 Simulated Time-Domain Results

Table 5. Test Flight Summary

CASE	FLIGHT	CARD	AAC	GAIN	NWS	FUEL (LB)	ALT (FEET)	MACH
19	140	4	OFF	15	2	8,311	19,005	0.5132
	140	4	OFF	20	3	8,077	18,930	0.5199
	140	4	OFF	25	4	7,887	18,942	0.5198
20	143	45	OFF	+3 dB	2	7,238	18,981	0.5237
	143	49	ON	+3 dB	2	7,125	19,031	0.5162
22	143	53	OFF	+3 dB	3	2,855	18,963	0.5236
	143	54	OFF	+6 dB	3	2,762	19,081	0.5154
22	144	54	OFF	+6 dB	3	6,149	18,874	0.5107
	144	54	OFF	+6 dB	4	6,040	18,911	0.5140
	144	54	OFF	+6 dB	2	6,000	19,072	0.5138
	144	54	OFF	+6 dB	1	5,940	19,047	0.5194
	144	58	ON	+6 dB	1	5,790	19,085	0.5177
	144	58	ON	+6 dB	2	5,565	19,131	0.5260
20	144	45	OFF	+3 dB	2	3,012	19,194	0.5210
	144	49	ON	+3 dB	2	2,875	19,137	0.5208
	144	46	OFF	+6 dB	2	2,682	18,976	0.5122

The total loop gain, in the presence of the airframe structural mode excitation, continued to be adjusted by the adaptive controller to suppress the otherwise unstable mode.

Figure 18 shows the results of TC 20 with AAC off and AAC on during Flight 143. The gray line in the upper left plot demonstrates the saturated state of the stabilator command due to limiting in the stabilator actuator system. The black line indicates the suppressed value of the stabilator command, as arrested by the decrease of total loop gain below unity shown in the bottom right plot. The upper right plot shows the spectral damper input, (sdamp) to the first order adaptive law continuing to arrest the growth of the mode in the control path. The oscillatory behavior of the adaptation response shown follows the trend as simulated prior to test (Figure 17) although the gain does not appear to decrease to the same extent. The difference in gain behavior may be due to the fact that the severity of the instability in flight may be less than predicted based upon the model fit or nonlinear behavior of the actuators near their maximum capability.

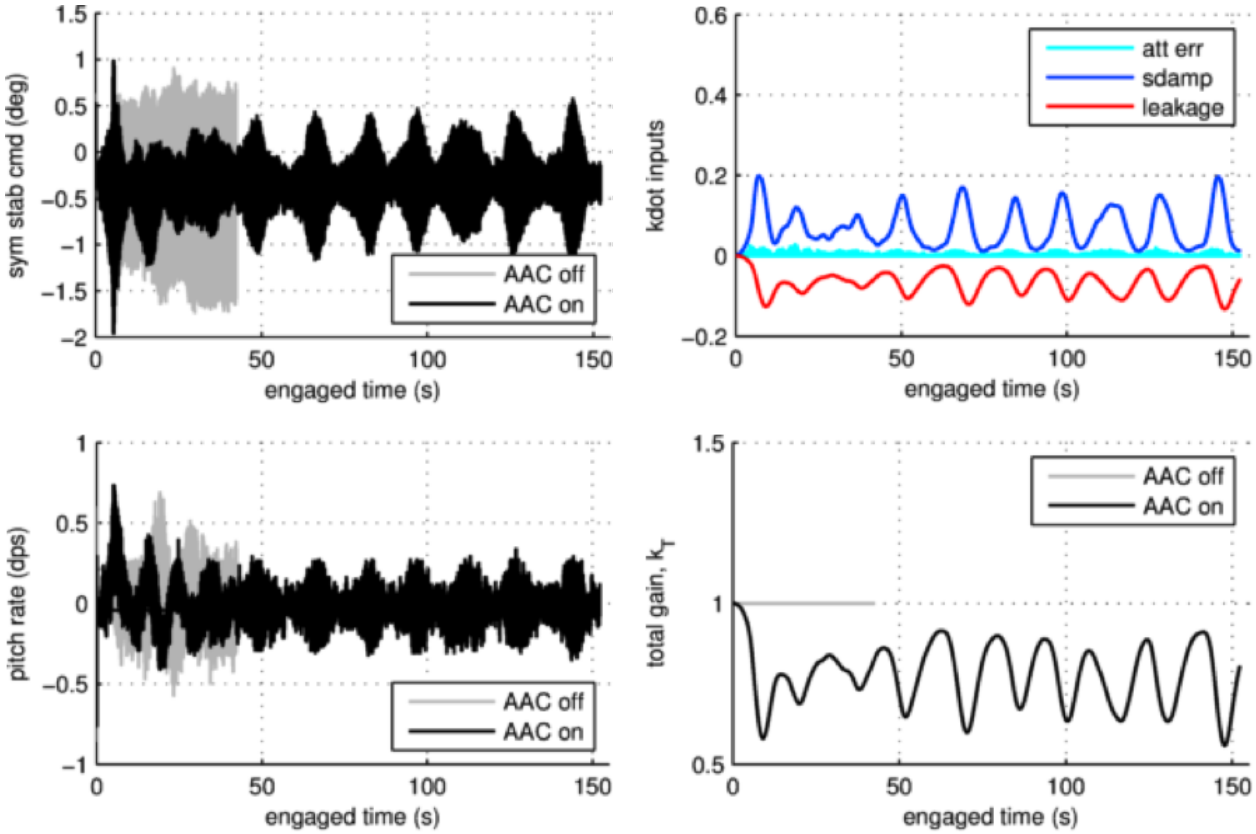

Figure 18. Test Case 20 Flight 143 Results

Figure 19 shows the results of TC 20 as flown at the very end of Flight 144. Despite being engaged with the exact same gain and phase settings as in Flight 143, the amplitude of the stabilator response is less for Flight 144. The adaptive gain decreases in response to the excitation, but to a lesser extent, indicating that the mode is either stable or is less unstable than in the Flight 143 test point.

Figure 20 shows the altitude, speed, and fuel level conditions for identification TC 19 and TC 20 runs in both Flight 143 and 144. While the altitude and speed conditions are all within variation of each other, the fuel level in Flight 144, being executed at the end of the research flight, is significantly further away from the conditions used to identify the modal response (TC 19 flown at the beginning of research Flight 140). The fuel-level condition, since it affects the total mass and mass distribution of the vehicle and, therefore, the structural dynamic characteristics, is the probable cause of the degraded performance for TC 20 in Flight 144.

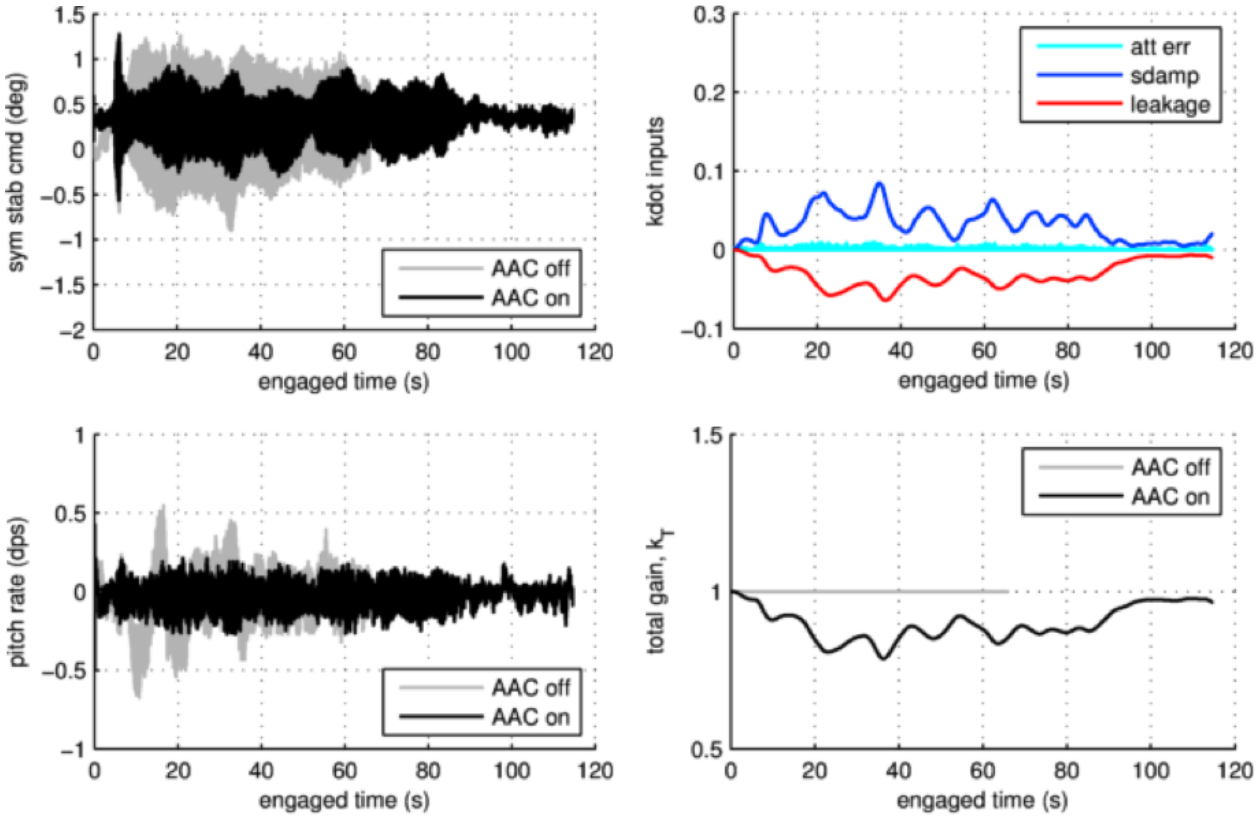

Figure 19. Test Case 20 Flight 144 Results

B. Flight Results for TC-22 (EGI sensor feedback)

TC 22, the modal amplification experiment utilizing the EGI sensor in the pitch rate feedback, was first attempted with the AAC off at the end of Flight 143 during the final return-to-base phase of the research flight. The conditions were set at a gain of +3 dB and three frame delays, corresponding to the mild level of stability as predicted in preflight simulations. When this test point showed very little excitation on the stabilators, a subsequent test point at the higher gain of +6 dB with the same three frame delays was engaged but still showed no apparent instability. This was the last test point taken on Flight 143, as fuel levels necessitated landing the aircraft.

The next test points for TC 22 were executed near the middle of Flight 144. The first of the Flight 144 (TC 22) runs were engaged with the same gain and delay conditions as the last point at the end of Flight 143 but again showed little excitation on the stabilators. At that state, since the gain was at the largest possible level of 6 dB, only phase adjustments were attempted. A second test point was engaged at +6 dB with four frame delays, which again showed little excitation on the stabilators. It was not until the third test point at a +6 dB gain with two frame delays that the stabilators started to show the limit-cycle behavior at 9.5 Hz. Finally, another test point was taken at +6 dB with one frame delay, and then the one and two frame delay test points were repeated with the AAC enabled. Figure 21 shows the symmetric stabilator command response of the various test points with the AAC disabled leading up to the two cases that resulted in instability (Flight 144, +6 dB, NWS 1 and 2). The bias offset between the Flight 143 and Flight 144 cases is due to the change in trim stabilator position required for the corresponding fuel condition. One possible explanation as to why less delay than predicted was required to bring the structure with EGI feedback to instability is that the EGI sensor used for modal identification was extracted from the telemetry stream which may have exhibited different delay characteristics than the signal connected to the ARTS for the amplification experiment.

Figure 22 shows the response of the TC 22 in the configuration with +6 dB gain and a single frame delay. Similar to the results for TC 20, when the AAC is disabled, the stabilator commands grow quickly to

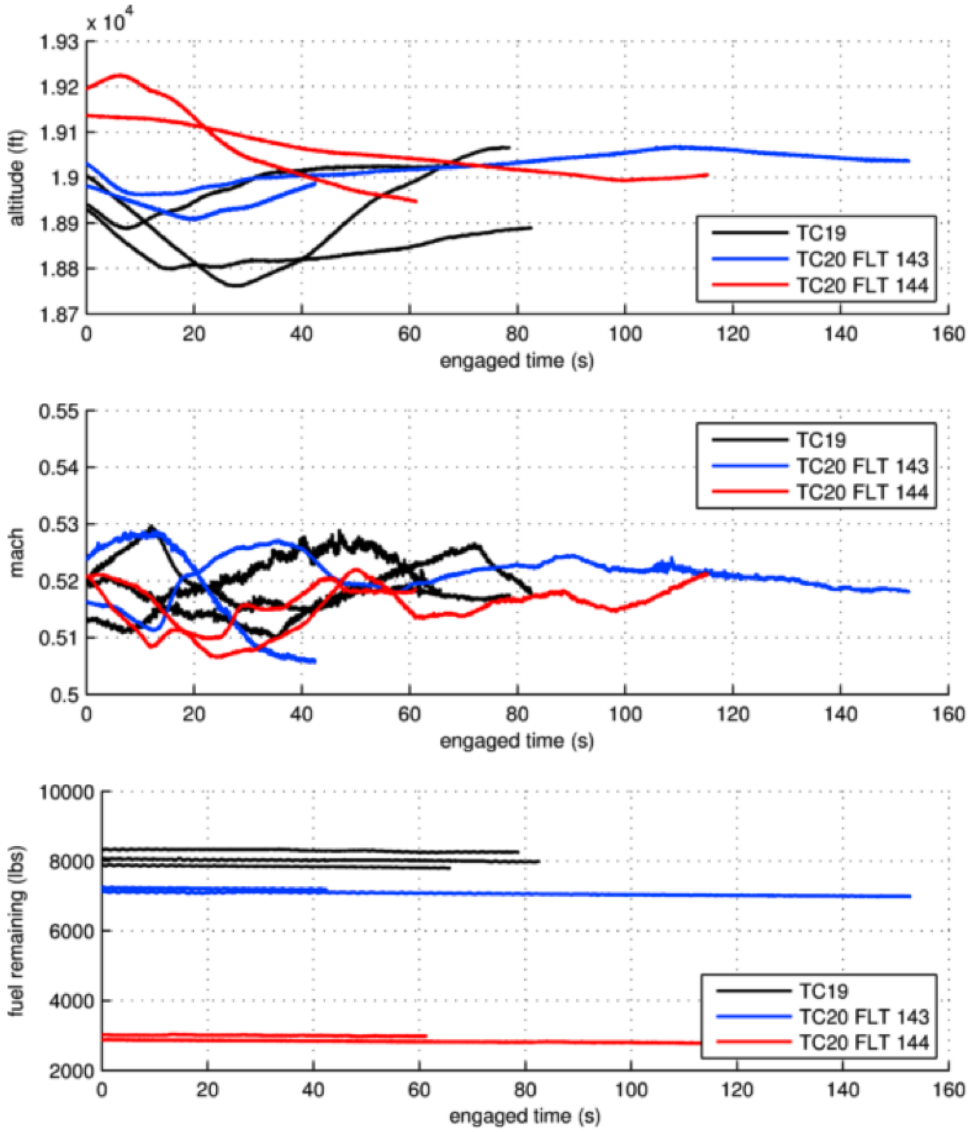

Figure 20. Test Case 19 and 20 Flight Conditions

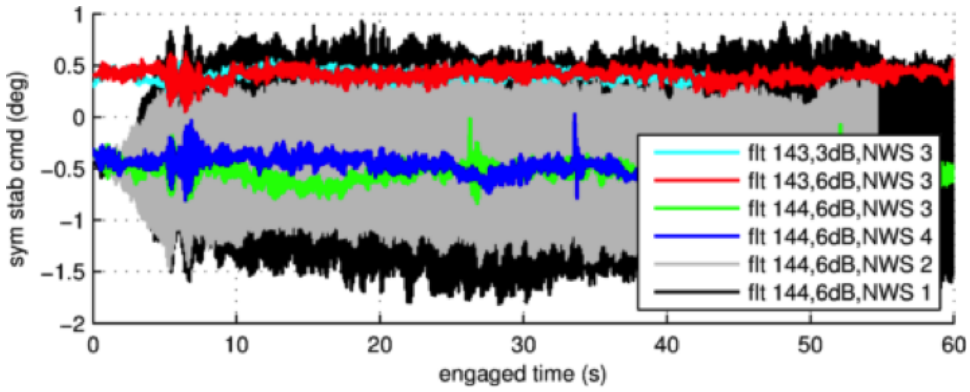

Figure 21. TC 22: Stabilator Cmd Responses in Search of Unstable Condition

a limit cycle oscillation constrained by the physical limits of their driving actuators. When adaptive control is enabled, the total gain decreases and reduces the amplitude of the response. Shown in bottom right plot, the high level of instability drives the adaptive controller to saturate the total gain at its lower limit with periodic upward excursions. A comparison of the saturated gain behavior in TC 22 and the smaller amplitudes in the TC 20 points indicates that the level of instability is more severe.

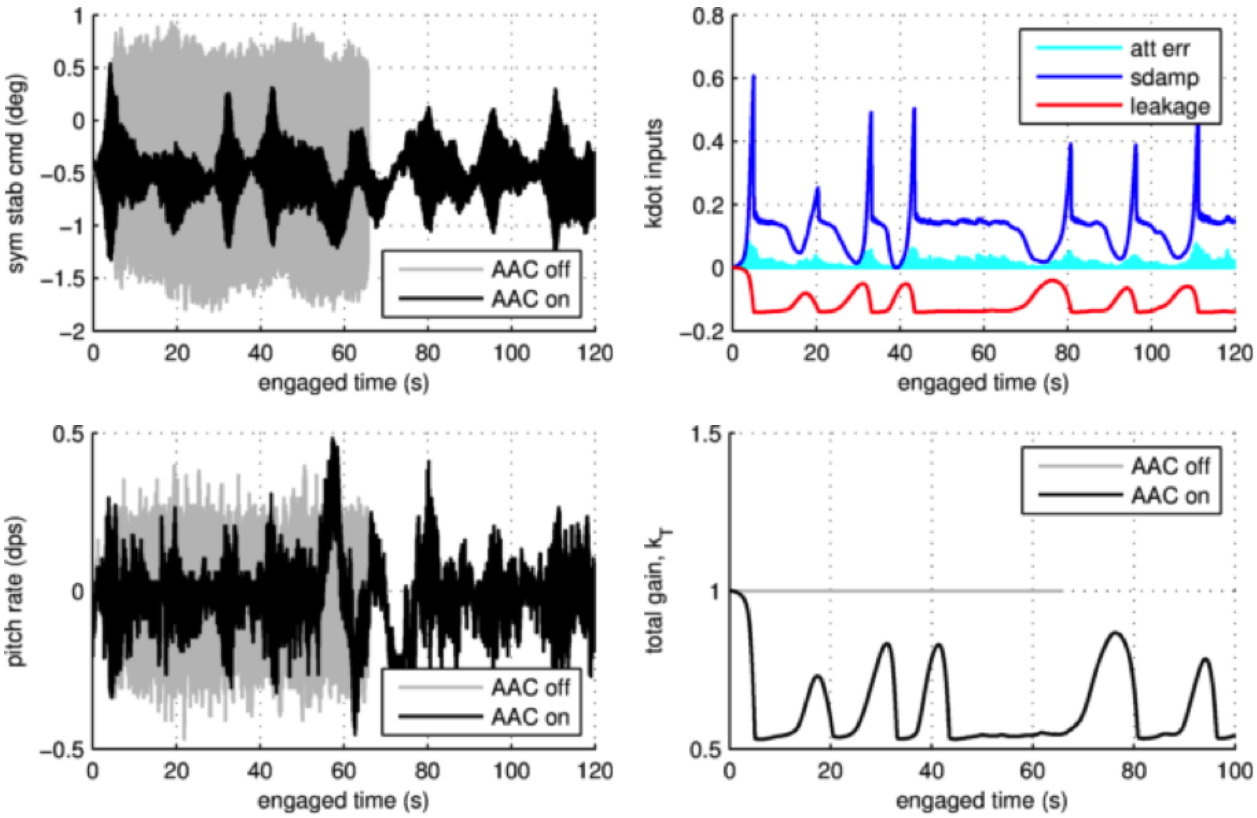

Figure 22. Test Case 22: 6 dB NWS 1 (0.0125s delay) Results

Figure 23 shows TC 22 with +6 dB gain and two NWS presses. The instability appears to still exist for this particular case as shown by the fixed stabilator command amplitude with the AAC off. However, a comparison of the total loop gain to the previously shown TC 22 indicates that a smaller gain decrease is required to arrest the unstable mode. The two gain decreases between 60 and 100 seconds correlate with the two swelled portions of the stabilator command and may be due in part to structural excitation from pilot adjustments to the trajectory to maintain speed and altitude.

Figure 24 shows the altitude, speed, and fuel level conditions corresponding to the TC 22 test points. The test points that achieved the desired unstable condition were flown in the middle of research Flight 144 and so were closer to the conditions for the modal identification TC 19 during Flight 140 than the late flight conditions in Flight 143. While further identification experiments are required to uncover the exact trend of the structural response with respect to fuel level, it is plausible that the half-fuel condition results in the maximum structural response. It is also possible that the bending gain at the EGI sensor location would show a different trend than the INS sensor location as a function of fuel level, due to the asymmetry of structural dynamics and mass distribution.

VI. Conclusions

Test cases were developed and executed during the LVAC research flights[1] that identified the fundamental mode of the F/A-18 airframe pitch axis structural response in the control loop, intentionally destabilized the mode, and demonstrated recovery of the instability with the SLS AAC algorithm. Test cases flown using pitch rate feedback from both the INS and the EGI sensors showed the expected behavior of the adaptive control algorithm as simulated and anticipated prior to flight. Sensitivity of the structural mode response to flight time was discovered during the flight campaign, and the closest match to preflight simulations was achieved when the fuel conditions for the amplification tests matched those used for system identification. Even with the differences between modeled and actual behavior, the AAC algorithm provided an appropriate level of gain compensation. This demonstrated the ability of the AAC algorithm to respond to an unexpected closed-loop structural instability.

VII. Acknowledgements

The authors wish to acknowledge the SLS Program, the NASA Engineering and Safety Center (NESC), and the Space Technology Mission Directorate (STMD) Game Changing Development Program (GCDP) for their support of this work. We would also like to thank the pilots Jim Less and David Larson and the many enabling contributions of the NASA AFRC, LaRC, and MSFC teams.

References

[1]VanZwieten, T., Gilligan, E., Wall, J., Orr, J., Miller, C., and Hanson, C., "Adaptive Augmenting Control Flight Characterization Experiment on an F/A-18," AAS Guidance, Navigation, and Control Conference, Breckenridge, CO, 2014.

[2]J. Orr and T. VanZwieten, "Robust, Practical Adaptive Control for Launch Vehicles," AIAA Guidance, Navigation, and Control Conference, Minneapolis, MN, August 2012.

[3]Wall, J., Orr, J., and VanZwieten, T., "Space Launch System Implementation of Adaptive Augmenting Control," AAS Guidance, Navigation, and Control Conference, Breckenridge, CO, 2014.

[4]Miller, C., "Nonlinear Dynamic Inversion Baseline Control Law: Architecture and Performance Predictions," AIAA Guidance, Navigation, and Control Conference, Portland, OR, 2011.

[5]Morelli, E. A., "Multiple Input Design for Real-time Parameter Estimation in the Frequency Domain," Paper REG-360, 13th IFAC Symposium on System Identification, Rotterdam, The Netherlands, August 2003.

[6]Orr, J., "Optimal Recursive Digital Filters for Active Bending Stabilization," AAS Guidance, Navigation, and Control Conference, Breckenridge, CO, 2013.

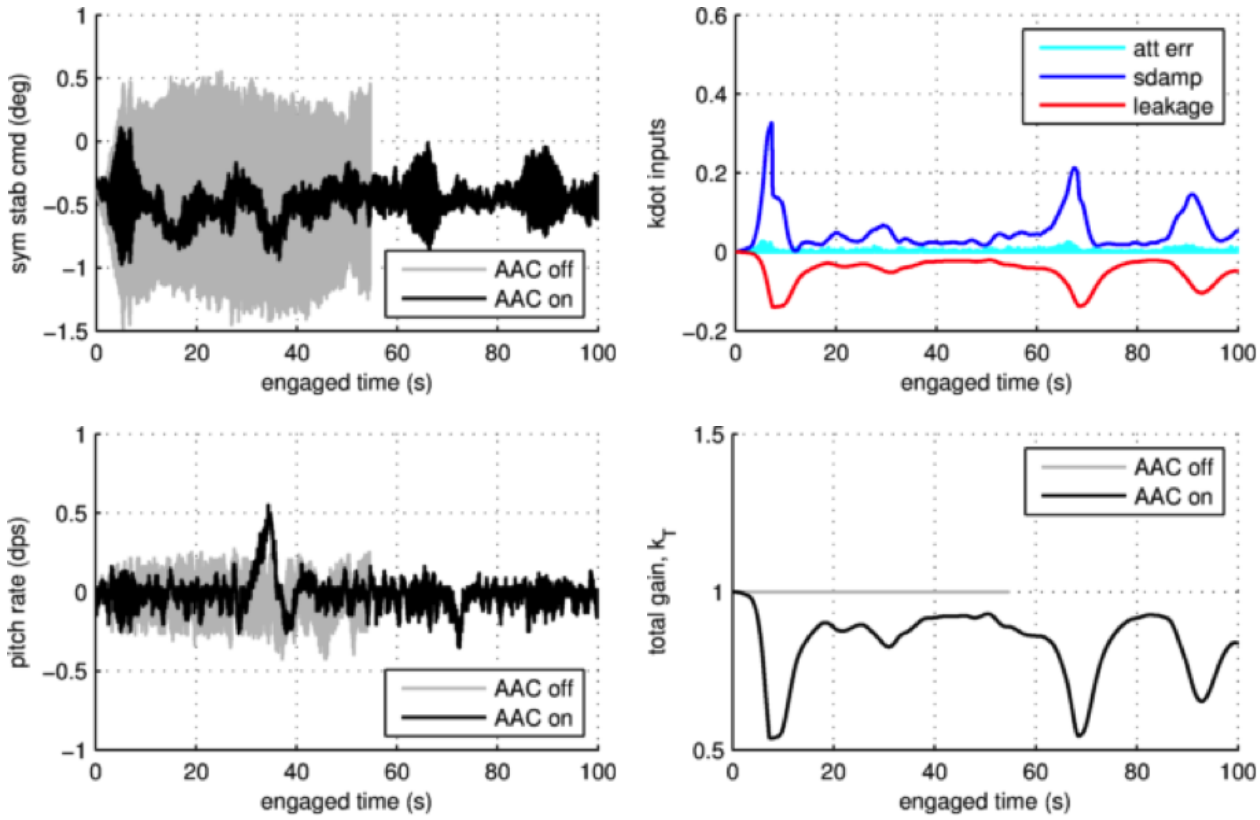

Figure 23. Test Case 22: 6 dB NWS 2 (0.0125s delay) Results

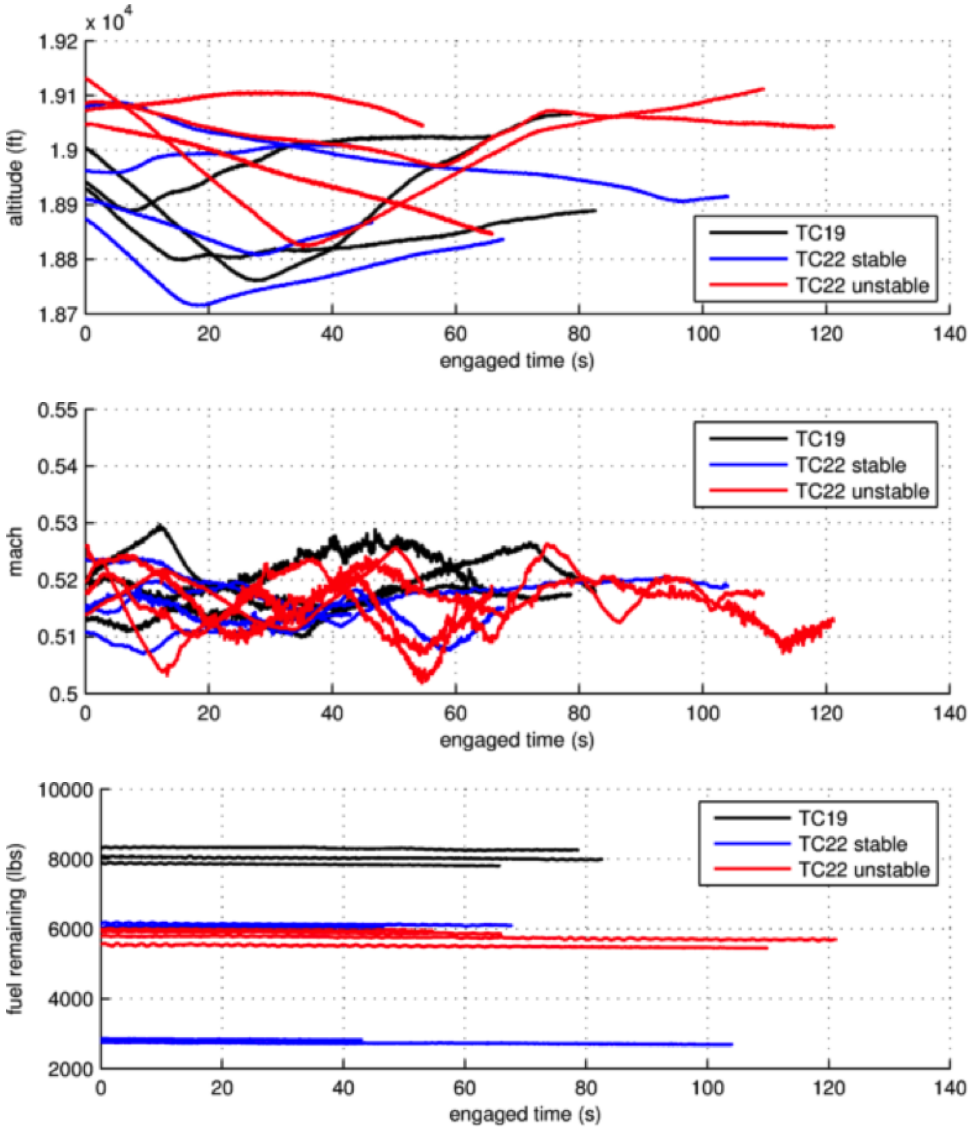

Figure 24. Test Case 19 and 22 Flight Conditions